Statistical study of magnetic cloud erosion by magnetic reconnection

A. Ruffenach,[1,2] B. Lavraud,[1,2] C. J. Farrugia,[3] P. Démoulin,[4] S. Dasso,[5,6] M. J. Owens,[7] J.-A. Sauvaud,[1,2] A. P. Rouillard,[1,2]A. Lynnyk,[1,2] C. Foullon,[8] N. P. Savani,[9,10] J. G. Luhmann,[11] and A. B. Galvin[3]

[1] Institut de Recherche en Astrophysique et Planétologie, Université de Toulouse (UPS), France

[2] Centre National de la Recherche Scientifique, UMR 5277, Toulouse, France

[3] Space Science Center, University of New Hampshire, Durham, New Hampshire, USA

[4] Observatoire de Paris, LESIA, UMR 8109 CNRS, 92195 Meudon, France

[5] Instituto de Astronomía y Física del Espacio, Buenos Aires, Argentina

[6] Departamento de Ciencias de la Atmósfera y los Océanos and Departamento de Física, Facultad de Ciencias Exactas y Naturales, Universidad de Buenos Aires, Buenos Aires, Argentina

[7] Space Environment Physics Group, University of Reading, UK

[8] EMPS/CGAFD, University of Exeter, UK

[9] George Mason University, Fairfax, VA, USA

[10] NASA Goddard, Greenbelt, MD, USA

[11] Space Sciences Laboratory, UC Berkeley, USA

Abstract. Several recent studies suggest that magnetic reconnection is able to erode substantial amounts of the outer magnetic flux of interplanetary magnetic clouds (MCs) as they propagate in the heliosphere. We quantify and provide a broader context to this process, starting from 263 tabulated interplanetary coronal mass ejections (ICMEs), including MCs, observed over a time period covering 17 years and at a distance of 1 AU from the Sun with Wind (1995-2008) and the two STEREO (2009-2012) spacecraft. Based on several quality factors, including careful determination of the MC boundaries and main magnetic flux rope axes, an analysis of the azimuthal flux imbalance expected from erosion by magnetic reconnection was performed on a subset of 50 MCs. The results suggest that MCs may be eroded at the front or at rear and in similar proportions, with a significant average erosion of about 40 % of the total azimuthal magnetic flux. We also searched for in situ signatures of magnetic reconnection causing erosion at the front and rear boundaries of these MCs. Nearly ~30 % of the selected MC boundaries show reconnection signatures. Given that observations were acquired only at 1 AU and that MCs are large-scale structures, this finding is also consistent with the idea that erosion is a common process. Finally, we studied potential correlations between the amount of eroded azimuthal magnetic flux and various parameters such as local magnetic shear, Alfvén speed, and leading and trailing ambient solar wind speeds. However, no significant correlations were found, suggesting that the locally observed parameters at 1 AU are not likely to be representative of the conditions that prevailed during the erosion which occurred during propagation from the Sun to 1 AU. Future heliospheric missions, and in particular Solar Orbiter or Solar Probe Plus, will be fully geared to answer such questions.

1. Introduction

MCs form a subset of Interplanetary Coronal Mass Ejections (ICMEs) characterized by clear signatures in the magnetic field and plasma parameters: an enhanced magnetic field strength, a large and smooth rotation in the magnetic field vector, a plasma with low proton temperature and a low proton β (the ratio between the proton thermal pressure and magnetic pressures) [*Burlaga et al.,* 1981*; Klein and Burlaga,* 1982]. The large-scale structure of MCs was first modeled as a force-free magnetic configuration with the geometry of a magnetic flux rope of circular cross-section [*Goldstein,* 1983*; Marubashi,* 1986*; Burlaga,* 1988*; Lepping et al.,* 1990]. As they propagate away from the Sun, MCs interact with the ambient solar wind. For instance, a leading shock may be driven by fast MCs with a sheath region forming between the shock and the front boundary of the MC [*Lepping et al*., 1990; *Gosling,* 1990].

McComas et al. [1998] suggested that these interactions could also include changes in the magnetic connectivity when, under favorable orientation, magnetic reconnection between the MC and the ambient Interplanetary Magnetic Field (IMF) takes places. It was then proposed that reconnection should peel off magnetic flux from the leading edge of the MC in such a way that the profile of azimuthal magnetic flux shows an imbalance across the structure. This erosion signature was illustrated in case studies by *Dasso et al.* [2006, 2007] and *Ruffenach et al.* [2012]. Based on pitch angle distributions of suprathermal electrons, *Ruffenach et al.* [2012] suggested that the "back region", which is the trailing part of the MC for which the counterpart at the front has been eroded, consists of field lines whose topology is different from the rest of the MC.

Magnetic reconnection has been detected at various boundaries in the solar wind [*Gosling et al*., 2005, 2006; *Phan et al*., 2006; *Lavraud et al*., 2009], including at the front of the MC studied by *Ruffenach et al*. [2012]. Locally this process is observed as a region bounded by two current sheets – i.e, a bifurcated current sheet – and so that magnetic field and flow disturbances are correlated at one boundary but anti-correlated at the other. Flow and field components at each current sheet satisfy the Walén relation, an expression of tangential stress balance. *Tian et al.* [2010] carried out a study of the occurrence of magnetic reconnection at the boundaries of 125 small-scale interplanetary magnetic clouds. These are modeled as flux ropes, akin to larger MCs, but typically of shorter duration (few hours) and with depressed proton density, and are observed mainly in the slow solar wind [e.g. *Cartwright and Moldwin*, 2008; *Feng et al.*, 2008]. They found that about 42% of the flux ropes have boundaries that exhibit signatures of magnetic reconnection.

MCs whose main axis lies in the ecliptic plane contain a strong southward IMF, either in their leading or trailing part, which often makes them strongly geo-effective [*Gosling*, 1990 *Farrugia et al*., 1997]. However, the impact of a geomagnetic storm may be affected by the erosion process, as it may remove a substantial portion of the magnetic flux that is oriented southward and opposite to that at the nose of the Earth's magnetosphere [*Lavraud et al.* 2014]. *Lavraud et al.* [2014] also highlight the fact that under favorable circumstances (for example with parallel magnetic fields in the MC and ICME sheath), enhanced compression associated with a lack of erosion increases MC geo-effectiveness.

The purpose of the present statistical study is to quantify the occurrence of MC erosion and to establish possible correlations with the properties of its environment. One main finding of our study is that erosion is apparently as likely to occur at the rear of MCs as at the front. In that regard, it may be noted that MCs are often followed and compressed by fast solar wind streams

[*Fenrich and Luhmann*, 1998; *Rouillard et al*., 2010], which may provide conditions favorable for erosion.

In section 2, we present the missions and datasets used. In Section 3, we examine all MCs observed during the solar cycle 23 by WIND and the two Solar Terrestrial Relation Observatory (STEREO) spacecraft, covering the period 1995-2012. In Section 4, we apply the method proposed by *Dasso et al.,* 2006 to analyze the imbalance in azimuthal magnetic flux for a selected subset of MCs, and we examine each boundary at the front and rear. In Section 5 we discuss the results.

2. Instrumentation

We use in-situ data from the WIND and STEREO missions. WIND magnetic field data are obtained with the MFI instrument [*Lepping et al.,* 1995] (3-s and 92-ms resolution) and plasma data with the 3DP instrument [*Lin et al.,* 1995] (3-s resolution).

We also use measurements from the STEREO probes [*Kaiser et al.,* 2008] that slowly drift ahead (referred to ST-A) and behind (referred to ST-B) the Earth on similar orbits around the Sun. The instruments onboard each of the two spacecraft are identical. We employ data from the magnetometers (MAG) [*Acuña et al.,* 2008] (3-s resolution) from the In Situ Measurement of Particle and CME transient (IMPACT) instrument suite [*Luhmann et al.*, 2008] and proton data from the PLASTIC instrument [*Galvin et al.,* 2008] (1-min resolution); SWEA suprathermal electron data [*Sauvaud et al*., 2008] were also often used to identify MC boundaries and reconnection exhausts.

WIND data were analyzed in Geocentric Solar Ecliptic (GSE) coordinates: **X**, **Y**, **Z**. For STEREO data, we worked in the RTN coordinate system: this system is centred on the spacecraft, **R** is the sun-to-spacecraft unit vector, **T** is perpendicular to it and points in the direction of planetary/spacecraft orbital motion, **N** completes the right-handed triad.

3. Magnetic Cloud Lists

We analyze MCs observed by WIND, ST-A and ST-B over 17 years from 1995 to 2012. We use the MC event lists compiled by *Lepping et al.* [2005, 2006] (http://lepmfi.gsfc.nasa.gov/mfi/mag_cloud_pub1.html) and by *Jian et al*. [2013] (http://www-ssc.igpp.ucla.edu/forms/stereo/stereo_level_3.html), respectively for WIND (1995-2008) and STEREO-A and B (2009-2012). *Lepping et al.* developed an automated method to identify MCs whereas *Jian et al.* analyzed each event visually. In both cases, the events combine a set of expected signatures, such as variation of magnetic field components, proton β and temperature. There is no overlap in the events and none of the MCs were sampled by both ST-A and ST-B.

MC boundary identification is a critical aspect for the proposed study both for computing magnetic flux imbalance and for searching for reconnection signatures. The interaction of MCs with their surrounding solar wind may lead to shocks and the formation of a sheath region with significant fluctuations in magnetic and plasma parameters. This often makes the determination of MC boundaries difficult [e.g., *Wei et al., 2003*], especially when the magnetic fields on either side of the boundary have similar orientations. Each MC was carefully inspected visually by combining a set of basic criteria specific to magnetic clouds: clear rotation of the magnetic field with a magnitude higher than the ambient solar wind, proton temperature lower than the average, β lower than 1, and nearby changes in pitch angle distributions of suprathermal

electrons. Start and end times are provided in the tables of the auxiliary material (column 1 and 2), together with other properties outlined below.

Some boundaries could not be determined with confidence; hence we categorized MCs as follows (column 4 in auxiliary material table):

- Quality 1 (Q1): front and rear boundaries are well determined;
- Quality 2F (Q2F): the front boundary is identified without ambiguity, but not the rear boundary. Conversely, for Quality 2R (Q2R) the rear boundary is the one we could properly determine;
- Quality 3 (Q3): both the front and rear boundaries are ambiguous and/or the structure does not exhibit clear MC signatures (unclear magnetic field rotation or complex internal structures such as shocks).

Figure 1 shows examples of MCs with quality 1 and 2F from WIND. The first MC (panel A, MC n°23, table WIND, Auxiliary Material) is a Q1. A clear large-scale rotation in the magnetic field components is observed within the MC. The proton temperature is below that in the surrounding environment, and significantly below the expected temperature as would be determined in the ambient solar wind from the empirical relation of *Lopez et al.* [1987] (shown by red trace). The proton β is lower than 1. The front boundary is determined on August 3 1997 at 13:52 UT. A large change in magnetic field direction is observed, along with a sharp decrease in the β and temperature. The rear boundary is also well determined at 2:03 UT on August 4, where we observe an abrupt change in the magnetic field components. It can be noticed that the velocity decreases from ≈500 to 410 km/s throughout the MC, and thus the radial expansion speed is approximated to V_{exp}≈*(500-410)/2=45km/s*.

The second MC in Figure 1 (panel B, MC n°54) is categorized as Q2F. The front boundary is well determined on August 12 2000 at 6:20 UT. At this time, the magnetic field magnitude increases, its components rotate and the proton temperature drops. The position of the rear boundary is more complex with weak variations of the magnetic field. In addition, two shocks are observed within the MC, around 1:00 – 2:00 UT on August 13. The presence of shocks and the ambiguity in the rear boundary determination thus make this case inappropriate for the study of azimuth flux imbalance. All MCs with either complex internal structures (e.g., shocks) or one of the two boundaries not properly determined are not appropriate for the study of flux imbalance. Our main results regarding flux imbalance will thus rely on Q1 MC, although we will also provide some results using Q2 MC for comparison purposes.

4. Analysis methods and signatures of erosion

4.1 Azimuthal magnetic flux imbalance

We first employ the method developed by Dasso et al. [2006, 2007] which consists in analyzing the variation of the accumulative azimuthal magnetic flux per unit length (L_{in}), defined as:

$$\frac{F_y(x)}{L_{in}} = \int_{t_{in}}^{t(x)} B_{y,cloud}(t') * V_{x,cloud}\, dt' \qquad \text{(Eq. 1)}$$

where t_{in} is the time of the MC front boundary, $B_{y,cloud}$ and $V_{x,cloud}$ are the respective components of the magnetic field and velocity in the MC frame and L_{in} is total length along the flux tube. The MC frame is defined [e.g., *Dasso et al*., 2006; *Ruffenach et al*., 2012] so that $\mathbf{Z_{cloud}}$ points along the main axis of the MC.

For MCs from Wind (STEREO) observations, we use GSE (RTN) coordinates. The direction

d is defined by the rectilinear trajectory of the spacecraft $\mathbf{X_{gse}}$ ($-\mathbf{X_{rtn}}$), $\mathbf{Y_{cloud}}$ is given by $\mathbf{Z_{cloud}} \times \mathbf{d}$, and $\mathbf{X_{cloud}}$ completes the right-handed coordinate system. Parameters θ and φ are defined in the GSE (RTN) coordinates as follows: the angle θ represents the latitude that is defined by the angle between the XY (RT) plane and the MC axis ($\mathbf{Z_{cloud}}$). The longitude φ is defined as the angle between the projection of MC axis on the ecliptic plane and the spacecraft-Sun direction (Sun-Spacecraft in RTN). The angles are positive when measured in a counterclockwise sense.

We compute the accumulative azimuthal flux by starting the integration of the component $B_{y,\,cloud}$ at the front boundary (cf. Figure 2b). As previously introduced, the appearance of an asymmetry in azimuthal flux may be interpreted as a signature of erosion by magnetic reconnection. As we analyzed the events, we found that for many cases the variation is incompatible with erosion at the front of the MC (as was deemed the case in *Ruffenach* et al. [2012]): the corresponding curve does not cut the abscissa before the rear boundary of the MC is reached, as illustrated in Figure 2a (MC n°10 in Wind Table, observed on July 1 1996). This suggests that erosion occurred primarily at the rear boundary; the excess magnetic flux is thus localized at the front of the MC. In such cases we thus start the integration at the rear boundary in order to determine the excess flux at the front, as shown in Figure 2a.

The orientation of the MC axis is a key parameter for estimating the eroded flux. For the present study, we employed the same methods as in *Ruffenach et al.* [2012], namely (1) minimum variance analysis (MVA) and (2) flux rope fitting (FRF).

(1) MVA

The MC main axis is computed using a combined "nested-bootstrap" MVA on the normalized magnetic field inside the MC (angle θ and φ in tables of Auxillary Material, columns 6 and 7). We apply a bootstrap method [e.g., *Kawano and Higuchi*, 1995] with 1000 random data resampling. We repeat this for 7 nested time intervals within the MC separated by 10 min: each of the 7 time intervals begins 10 min after the previous and ends 10 min before. This resampling technique is meant to assess the impact of magnetic field intrinsic variability on the main MC axis determination and, in turn, the impact on the imbalance in azimuthal magnetic flux.

(2) FRF

Flux rope fitting is also employed to provide a second estimate of the axis orientation. However, as explained in section 6, the associated results and analysis are not presented in detail. Since MCs may be characterized by a radial expansion (speed profile inside MC decreases gradually, e.g., MC in panel A of Figure 1), we modified the fitting procedure employed in *Ruffenach et al.* [2012]. Several methods have been developed in order to take the dynamic evolution of MC into account. We use a force- free model based on a cylindrical geometry with a self-expansion in the radial components (by fitting a model to the velocity radial component) [*Farrugia et al.,* 1993]. Then, the Lundquist [1950] solutions are modified to take the temporal evolution of the MC into account. We specifically utilize the procedure described in *Nackwacki et al.* [2008]. The output parameters are: axis orientation, impact parameter (Auxiliary Material Tables column 11) (i.e, the closest distance between the center of the flux tube and the spacecraft trajectory, which is approximated as an initial guess by $\langle B_{x,cloud}\rangle/\langle B\rangle$, Auxiliary Material Tables column 10, where $B_{x,cloud}$ is computed in the MC frame previously obtained from MVA [*Démoulin and Dasso*, 2009]), magnitude B_0 and helicity of the magnetic field (Auxiliary Material Tables column 12). We use the Levenberg-Marquardt algorithm, which numerically minimizes problems in least squares curve fitting for the multiple

variables involved.

The accumulated azimuthal magnetic flux is then computed by starting the integration of the B_y component (in Eq. 1) both at the leading and at the rear MC boundary (Figure 2). The estimate of the total azimuthal magnetic flux ($F_{t,azimuthal}$) (per unit of length) before reconnection corresponds to the sum of F_y/L (in absolute value) chosen between the peak of the accumulated flux and the value at rear boundary of the MC, when the azimuthal flux variation is compatible with erosion at the front (cf. Figure 2b). If it is the rear that has been eroded, $F_{t,azimuthal}$ is the sum computed between the peak of the accumulated flux and the value at the front boundary (curve profile *of* $F_{t,azimuthal}$ is reversed as in Figure 2a). The eroded azimuthal flux $F_{e,azimuthal}$ (i.e., equal to the azimuthal flux contained in the back/front region) is given by the absolute value of F_y at the MC rear boundary (or at the front is eroded at rear). The computation of $F_{t,azimuthal}$ is performed assuming $p=0$, where p is the impact parameter. These values of the total azimuthal flux are thus lower estimates of the actual value when p is large (as further discussed later). Moreover, we only focus on the azimuthal flux variations in this study because it is one order of magnitude larger than the axial flux [*Mandrini et al., 2007*, *Dasso et al., 2007*] and erosion mainly affects the outer parts of the MCs where azimuthal flux dominates.

As an example, the black curve in Figure 2b displays the $B_{y,cloud}$ component in a MC frame deduced from the mean axis orientation obtained from all the MVA bootstrap results. The variation of the azimuthal flux is, for this event, consistent with front erosion and the estimated amount of eroded azimuthal flux is 31 (±13) % (mean value from all generated curves with standard deviation). Values of the amount of eroded azimuthal flux rate at the front (or rear) are indicated in column 15 of the auxiliary material tables, with the corresponding standard deviation. Negative values correspond to front erosion and positive values to rear erosion. For some events the estimation of the amount of eroded flux is inconsistent with either erosion at the front or at the rear (28%-38%-50% of total events observed respectively by Wind, ST-B, ST-A), e.g., $B_{y,cloud}$ never changes sign, which indicates that the MC main axis was not well determined (missing values in columns 13, 14, 15 of Auxillary Material Tables).

4.2 Magnetic reconnection signatures at MC boundaries

MC erosion implies that magnetic reconnection has occurred locally at the front and/or rear boundaries during propagation [*McComas et al*., 1988 ; *Dasso et al*., 2006 ; *Möstl et al*., 2008 ; *Tian et al*., 2010 ; *Ruffenach et al.*, 2012]. The in-situ observation of a pair of rotational discontinuities embedding an alfvénic plasma jet is often used as a signature of magnetic reconnection in the solar wind [e.g., *Gosling et al*., 2005, 2011].

We examine each well-determined boundary (from the Q1/Q2R/Q2F MCs) to make an inventory of such signatures. Since the Wind data resolution is sufficient, we applied the Walén Test [*Hudson*, 1970 ; *Paschmann et al*., 1986] to this MC list at boundaries where clear bifurcated current sheets are found (cf. also *Phan et al.* [2006] or *Ruffenach et al*. [2012]):

$$V_{pre} = V_{ref} \pm \rho_{ref}^{1/2} \times (B/\rho - B_{ref}/\rho_{ref}) / \mu_0^{1/2} \quad \text{(Eq 2.)}$$

Here, V, B, ρ, represent the velocity, magnetic field and density (the pressure anisotropy factor is not accounted here owing to the lack of such data). The subscript "ref" denotes the reference time at the leading or trailing edge of the exhaust in the upstream region, and subscript "pre" denotes the velocity predicted across the region for an exhaust bounded by rotational discontinuities. The positive sign is used at one current sheet of the exhaust, and the negative sign at the other. The order depends on the crossing of the spacecraft relative to the X-

line location.

However, due to lower resolution plasma measurements, STEREO data typically did not permit to perform the Walén test. Therefore, we made a classification of observed reconnection signatures as follows.

- Wind data set:

- Category 1: correlations between magnetic and velocity components at one end of the bifurcated current sheet are opposite to those at the other end. A flow enhancement is observed inside the bifurcated current sheet, and the quantitative correlation between observed and predicted (Walén) velocity components is good.
- Category 2: correlation between the predicted (Walén) and observed velocity components is good for one current sheet, but a significant discrepancy is found for the other despite a clear change. The other signatures (presence of a flow enhancement and bifurcated current sheets) are observed.
- Category 3: Although correlation / anti-correlation are observed for magnetic and velocity components, data resolution is insufficient to apply the Walén test.

All other cases show no signatures of reconnection, which is deemed to be absent locally at the boundary.

- STEREO-A and B data sets:

The Walén test cannot be carried out in the majority of cases owing to the insufficient time resolution and frequent absence of proton velocity components. We thus rely on magnetic reconnection signatures which are classified as follows.

- Category 1: a bifurcated current sheet with flow enhancement is observed, and the velocity components show variations consistent with the expected correlation/anti-correlation at the two successive current sheets (but, again, a quantitative Walén test could not be performed on all components).
- Category 2: a bifurcated current sheet is observed. However, missing data and/or insufficient resolution in proton velocity components prevents us from determining the presence of a flow enhancement.

For all other cases the magnetic field does not show bifurcation, and no flow enhancement is observed. Magnetic reconnection is deemed to be absent. These criteria, for determining if magnetic reconnection signatures are present, are summarized in the auxiliary material tables (columns 16 and 17).

Figure 3 illustrates different signatures as observed by Wind, and belonging to these different categories. Each case corresponds to a zoom on a given MC boundary (at the front or rear). Each panel shows from top to bottom (a) density, temperature, (b) magnetic field components (92-ms resolution) and (c-e) velocity components (3 sec.), in the GSE coordinate system. Black dotted lines delimit the reconnection exhaust intervals.

For the category 1 case (first set of panels), the boundary is first characterized by a rotation in B_x and B_z. Magnetic field and velocity components are anti-correlated at the first current sheet and correlated at the second. A plasma enhancement is observed in ΔV_x (nearly *45 km/s*) and V_z (*45 km/s*). The Walén Test is performed for the interval indicated between green vertical dotted lines and we observe an excellent correlation between predicted (colored dotted curves) and observed velocity components. These elements confirm the presence of a magnetic reconnection exhaust at this MC boundary.

For the category 2 case (second set of panels in Figure 3), a rotation in the magnetic field is

observed adjacent to a plasma enhancement ($\Delta V_z \sim 80km/s$). The observed velocity is consistent with the predicted one at the first current sheet (Walén test). Despite the direction being correct, the predicted velocity change at the second current sheet is not as good in V_x and V_y: the expected variations are much larger than the observations. We note that this particular boundary is highly asymmetric, with significantly different densities (from *13* down to *3* cm^{-3} over the interval shown) and magnetic field magnitude on each side. The Alfvén speed is thus extremely high on the right-hand side. We speculate that the overestimation of the predicted velocity in the Walén test has to do with this strong asymmetry. Recent work suggests that plasma flows in reconnection exhausts may be linked to a 'hybrid' Alfvén speed [cf. *Borovosky and Hesse*, 2007], while the basic Walén test used here supposes plasma velocity follows the local Alfvén speed. In this case we also note a small-scale structure at the second current sheet. It makes this case more complex than regular reconnection exhaust, and may affect our definition of the outside reference point for the Walén test. Since in addition all other signatures are consistent, it is quite probable that this category 2 case is an actual reconnection exhaust.

A category 3 case is presented in the third set of panels in Figure 3. We identify a bifurcated structure together with a flow enhancement (around $\Delta V=20\ km/s$). However, the resolution of the velocity data is low and does not permit a meaningful Walén test. Yet the successive increase and decrease in the V_Z components are consistent with Walén predictions, as shown by the dotted lines in the velocity panels. In particular the main plasma flow change is observed in the V_Z component, compatible with the main magnetic field change which is also in the B_Z components at the current sheets. This case is also likely the remnant of a reconnection exhaust [e.g., *Foullon et al*. 2009].

5. Statistical Results

First, we analyze the distribution of the amount of eroded azimuthal magnetic flux and attempt to correlate this with the properties of the surrounding solar wind environment. We then examine magnetic reconnection signatures observed at the front and rear boundaries.

5.1 Selection criteria

In Section 3, we mentioned that to investigate azimuthal magnetic flux imbalance it is necessary to classify MCs with respect to boundary identification. Thus, we do not take into account MCs of quality 3 for which the positions of both the front and rear boundaries are uncertain. We will only use MCs of quality 1, and where appropriate, those of Quality 2 as explained later. The computation of the azimuthal magnetic flux also requires accurate knowledge of the MC axis orientation. We thus made further selection of the MC quality based on another set of criteria related to the axis determination.

On the one hand, *Gulisano et al.* [2007] highlights the fact that the axis orientation is well determined with MVA when its inclination is close to the ecliptic plane and the impact parameter is small. On the other hand, when the intermediate-to-minimum (λ_2/λ_1) or maximum-to-intermediate (λ_3/λ_2) eigenvalue ratios from MVA are lower than 2, the eigenvectors are close to being degenerate [cf. *Sonnerup and Scheible*, 1998] and consequently the MC axis is poorly determined. Also, the application of the nested-bootstrap method on MVA sometimes shows significant uncertainties in axis determination owing to substructures in MCs. This leads to errors in azimuthal flux imbalance estimates (cf. all curves generated in Figure 2) that we quantify with the computation of the standard deviation for θ and φ. We found that for values of

$\Delta\theta$ and $\Delta\varphi$ greater than 15°, the scattering becomes particularly significant so that flux imbalance estimates are deemed unusable.

The flux rope fitting is also impacted by various errors: magnetic field fluctuations inside the MC [*Janoo et al*., 1998], incorrect boundary selection, or non-circular MC cross section [*Savani et al*. 2011a, b]. Also, when the impact parameter is high, the MC structure is not clearly identifiable as a cylindrical structure [e.g. *Riley et al., 2004*, *Démoulin et al.,* 2013, *Savani et al.* 2013].

Finally, we add a geometrical criterion related to the fact that azimuthal flux variations are biased when the spacecraft crosses the leg of the MC. Figure 4 shows various crossings inside a non-eroded MC in the plane containing its axis. The MC is modeled with a force-free field where the flux tube is in the ecliptic plane and curved according to a Parker spiral (cf. *Owens et al.* [2012]). For each trajectory, the angle α between the normal at the axis orientation to the trajectory is gradually increased (0°, 32°, 57°, 62° respectively for the trajectories A, B, C, D) as illustrated in Figure 4a. The magnetic field vector is generated and we apply MVA to determine the magnetic field components in the MC coordinate system, and integrate *By*. We then compute the accumulative azimuthal magnetic flux. The corresponding amounts of eroded magnetic flux are summarized in Figure 4c. For trajectory A, the crossing is perpendicular to the MC axis. The B_y component is completely symmetric and the associate curve of the accumulative azimuthal magnetic flux cuts the axis exactly at the rear boundary. However, for higher values of the angle between the trajectory and the normal, B_y becomes asymmetric. This demonstrates that, despite the fact that the present model does not account for any type of erosion process, the trajectory of the spacecraft crossing (i.e., in the fashion of a MC leg crossing) can lead to asymmetries in azimuthal magnetic flux which may be misinterpreted as the result of erosion. This apparent flux imbalance stems from the axis bending. There is a systematic effect so that it is always the rear part of the MC which has more flux. We note, however, that false erosions larger than 10 % only occur for angles greater than 45°.

To account for this effect, we note that the MC axis determination gives implicit information about the spacecraft trajectory orientation through the MC. *Janvier et al*. [2013] introduced two new angles to define axis orientation, which are presented in Figure 5: the angle i is the inclination angle of the MC axis to the ecliptic plane, and the angle λ evolves along the flux rope and indicates whether the spacecraft crosses a MC leg (if the axial shape is known to be regular). Following the modeling of Figure 4 for a MC axis in the ecliptic plane, we estimate that λ values included between ± 45° correspond to a S/C trajectory sufficiently close to the apex so that errors on the azimuthal flux imbalance should be lower than 10%.

Based on the above arguments, we used the following criteria to select a proper subset of MC for our analysis, for both results using MVA and FRF:

• Group MVA:

1. Quality 1 MC
2. Ratio λ_2/λ_1 and $\lambda_3/\lambda_2 > 2$,
3. $\Delta\theta$ et $\Delta\varphi < 15°$
4. $\lambda < |45°|$
5. Impact parameter $p < 0.6$

• Group FRF:

1. Quality 1 MC

2. Impact parameter $p < 0.6$
3. $\lambda < |45°|$
4. Fitting method converges.

Groups MVA and FRF respectively comprise 50 and 30 events (WIND, STEREO-A and B lists combined).

5.2 Analysis of azimuthal magnetic flux imbalance.

The results for group "MVA" suggest that 46 % of the MCs are eroded at the front and 54 % at the rear. Figure 6a presents the distribution of the amount of eroded azimuthal magnetic flux, normalized to the estimated total azimuthal magnetic flux in the MC (in %). MCs eroded at the front are plotted on the left in the range -100% to 0%. Those eroded at the back are in the range 0% to 100 %. In absolute value (Figure 6b), i.e. not making the distinction between front and rear, the distribution decreases gradually but yet shows a significant average value of 46% erosion for the present set of MCs. We recall that the total azimuthal flux is underestimated for impact parameters p > 0, so that the amounts of erosion (in % relative to the total azimuthal flux of the MCs) reported should be viewed as upper estimates.

Compression processes (at the front or rear of MC) may play a key role in MC erosion. Indeed, compression in the sheaths of MCs, for instance, leads to an increase in Alfvén speed at the MC boundary, which will enhance the reconnection rate if reconnection is ongoing. Because compressions are driven by flows, we analyzed the amount of azimuthal eroded flux with respect to the MC (Figure 7a) and ambient solar wind (Figure 7b) speeds. The ambient solar wind ($V_{sw,front}$) here is the local measurement of proton speed at the MC front. This value was selected by eye ahead of the front boundary or before the shock/sheath if present. Neither plots show obvious correlations. We then analyzed potential correlations between erosion and the speeds across the front and rear boundaries, keeping in mind the possible role of compression process. The results are presented in panels c and d of Figure 7. The computation of ΔV_{front} corresponds to the difference between the average of the MC speed in its first 5% (time wise, in order not to be biased by the MC expansion) and $V_{sw,front}$ ($\Delta V_{front}=V_{MC}-V_{sw,front}$, with $V_{sw,front}$ still ahead of the shock if present). For ΔV_{rear}, we calculate the difference between the MC speed (last 5% in trailing part of the MC) and the velocity of the solar wind at the rear. The procedure to compute $V_{sw,rear}$ is different: based on 30 min averages we use the highest speed in the 6 hour interval following the MC. In Figures 7a-d correlations were searched both across all erosion values and separately for front (-100 – 0%) and rear (0 – 100%) erosions (because it is not necessarily meaningful to try to correlate these various parameters throughout all values of erosion). However, regardless of such issues, our dataset does not show any obvious correlation.

Since the reconnection rate scales with the local Alfvén speed, we also investigated potential correlations with the Alfven speeds measured at the MC boundaries. *Cassak and Shay* [2007] used conservation laws to derive a hybrid Alfvén speed which should relate to the reconnection rate in the case of asymmetric reconnection. Assuming antiparallel reconnection between plasmas of different magnetic field strengths and densities, they defined (in MKS units):

$$V_A = \sqrt{\frac{B_1 B_2}{\mu_0 \rho_0}}$$

With:

$$\rho_0 = \frac{B_1\rho_2 + B_2\rho_1}{B_1 + B_2}$$

Here B_1 and B_2 (ρ_1 and ρ_2) are, respectively, the magnetic field strengths (densities) averaged over 15-minute intervals adjacent to the boundaries, and ρ_0 is the density in the outflow region. The amount of erosion as a function of the local hybrid Alfvén speed at the MC boundary (front boundary for front erosion and rear boundary for rear erosion) is displayed in Figures 7e and 7f. Again, no meaningful correlation is observed for the local hybrid Alfvén speed. Although not shown, we have also investigated the correlation with the local magnetic shear, as well as with a hybrid Alfvén speed that is a function of the magnetic shear. But again no correlations were found. As further discussed in section 5, this lack of correlation may be explained by the fact that erosion occurs all the way from the Sun to the Earth, so that local measurements at 1 AU may be unrelated to what occurred earlier during propagation.

This analysis was also performed for Group FRF, based on results from FRF. It is not detailed here but again no relationships were found. We noticed, however, a major difference in the distribution of the amount of eroded flux, which is explained in section 5.

Due to our stringent selection criteria, both subsets A (50) and B (30) contain a relatively low number of events as compared to the total number of MCs observed by Wind and STEREO lists. We thus performed all the analyses on various other subsets, for instance by including all MCs of Category 2 or releasing the criteria on p or λ, but again no correlations were found. In the tables results are given, for example, for the subsets called MVA* and FRF*, defined as:

• Group MVA*: (87 MCs)
1. Quality 1 and 2 MC
2. Ratio λ_2/λ_1 and $\lambda_3/\lambda_2 > 1.5$,
3. $\Delta\theta$ et $\Delta\varphi < 15°$
4. $\lambda < |60°|$
5. impact parameter $p < 0.8$

• Group FRF*: (89 MCs)
1. Quality 1 and 2 MC
2. Impact parameter $p < 0.8$
3. $\lambda < |60°|$
4. Fitting method converges.

5.3. Magnetic reconnection signatures

Now we give the results of our search for magnetic reconnection signatures at MC boundaries. Since we care about the occurrence of erosion from magnetic reconnection at their outer boundaries, we only study boundaries whose identification is well-established. We thus analyzed all boundaries of MCs of quality 1, 2F (front boundary) and 2R (rear boundaries). The Tables in the Auxillary Material (columns 16 and 17), give the number of signatures observed, classified according to criteria described in section 3.

- WIND Data:

Of the 83 front boundaries examined, 15 signatures consistent with magnetic reconnection (categories 1, 2 and 3) were observed. Thus, 18% of the front boundaries show signatures of magnetic reconnection. Of the 60 rear boundaries examined, 17 signatures (categories 1, 2 and 3) of magnetic reconnection were found (28%). This gives an average of ~22% on all

boundaries.

- STEREO-A:

We examined 42 front boundaries and 38 rear boundaries. For front boundaries 11 category 1 signatures were found; 27 with category 1 and 2 signatures. Numbers are 10 (category 1) and 22 (category 1 and 2) for rear boundaries. Hence, the frequency of magnetic reconnection signatures is in the ranges 26-64 % at front boundaries, and 26-58 % at the rear.

- STEREO-B:

We examined 46 front boundaries and 34 rear boundaries. For front boundaries 16 category 1 signatures were found; 24 with category 1 and 2 signatures. For the rear boundaries, 9 and 17 events were found for category 1 and categories 1 and 2, respectively. Hence, the frequency is included the range 35-52 % at the front, and 26-50 % at the rear.

6. Discussion

The purpose of this study is to quantify two key signatures of the erosion process at the front or rear of MCs: (1) the imbalance in azimuthal magnetic flux and (2) signatures of local magnetic reconnection. Our first main finding is that erosion as suggested from azimuthal magnetic flux imbalance occurs both at the front and rear boundaries and in similar proportions (groups MVA and MVA*).

For group MVA (axis orientation is determined with MVA), 23 MCs are eroded at the front and 27 at the rear, with the amount of eroded azimuthal magnetic flux being 42 % for MC eroded at their front ($1.07*10^{21}$ *MX/AU* of flux eroded) and 32.8 % for MCs eroded at the rear ($0.9*10^{21}$ *MX/AU* of flux eroded). Concerning the subset MVA* (with less restrictive criteria), the results are similar. It should be noted that the dispersion of the results are significant, highlighting the variability inherent in the methods and selection process (standard deviation σ is indicated in brackets in Table 2, with the uncertainty on the average $\sigma/\sqrt{(n)}$ where n is the size of the sample).

In Table 2 we also present the results for group FRF and FRF* (MCs whose axis orientation is determined with FRF). We clearly note that the amount of eroded azimuthal magnetic flux for these groups are lower: 24 % for front erosion and 28.4 % for rear erosion for group FRF, and respectively 23.3 % and 30.6% for group FRF*. This systematic difference between groups MVA and FRF may stem from the method employed to estimate the axis orientation. Figure 8 compares the amounts of eroded azimuthal magnetic flux (without distinction between erosion at the front and at the rear) found between the two methods used for axis orientation determination (groups MVA and FRF), for MCs which are in both groups. We notice that when the axis orientation is determined with FRF, the erosion is systematically underestimated by nearly 33%**.** This value reaches 40 % when groups MVA* and FRF* are analyzed.

FRF is based on the assumption of a circular cylindrical geometry, so that the underlying model has an axis of symmetry. So in fact applying this model on an eroded structure, which is asymmetric by definition, constitutes an inconsistency. The reader is referred to Figure 1 in *Ruffenach et al.* [2012] where these symmetry/asymmetry issues are addressed. Fitting MC magnetic field components with Lundquist solutions thus forces the result to be symmetric, which is consistent with the tendency of this method to find systematically lower values of the erosion. The method is thus not appropriate for the reconstruction of eroded MCs. It must be noted that if erosion is large, the determination of the axis by MVA will also be altered, although possibly less than with FRF as is suggested by the clear trend observed in Figure 8.

We have, however, no means of quantifying the impact on erosion estimates through the direct method of *Dasso et al.* (2006; 2007). This limitation adds to the fact that the total azimuthal flux of the MCs is underestimated by this method when impact parameters are large, and suggests that the estimates of the relative amounts of erosion (in %) given here should be viewed as upper limits (with added significant uncertainties intrinsic to the method; cf. column 15 of auxiliary material tables). Future studies, when larger MC datasets are available, will be necessary to disentangle these possible biases.

Despite these limitations, we searched for possible correlations between the amount of eroded azimuthal magnetic flux (front or rear) and various parameters (Figure 7). We did not find any. In particular, we did not find any trend between the amount of erosion and the MC speed, ambient solar wind speed, or their changes at the front and rear boundaries. This lack of trend may be surprising since compression processes at either the front or rear may increase the local Alfvén speed, and in turn the local reconnection rate. However, this may be explained by the fact that most of the erosion is thought to occur in the inner heliosphere, typically inside of Mercury's orbit [*Lavraud et al*., 2014]. No trends were found when analyzing parameters such as the local hybrid Alfvén speed or local magnetic shear either. Similarly, such lack of correlation may simply result from the fact that measurements made locally at 1 AU are typically unrelated to the conditions that prevailed during propagation in the inner heliosphere, and that potentially controlled most of the erosion process.

Regarding local magnetic reconnection signatures at MC boundaries, it was necessary to classify them. The Walén test could only be performed on Wind data, which has sufficient temporal resolution over what are typically short time intervals. For MCs with well determined boundaries, we note the frequent observation of local magnetic reconnection signatures, in the range 20 to 50% depending on spacecraft and criteria. These results are compatible with the rate of 42% found at boundaries of small flux ropes by *Tian et al.* [2010]. Thus, magnetic reconnection is common at MCs boundaries at 1 AU. We may further note that reconnection is expected to be even more frequent in the inner heliosphere, thanks to a higher probability of the occurrence of a low plasma β [*Swisdak et al*., 2010]. The observed large occurrence of reconnection signatures at the boundaries of MCs is compatible with the significant amount of erosion statistically found based on the imbalance of the azimuthal magnetic flux imbalance within MCs.

Finally, we note that only 41% of MCs (MVA* group) eroded at the front showed evidence of local reconnection signatures at the front boundary, and similarly only 36% for the rear boundary. This is in fact not unexpected since the observation of reconnection locally at 1 AU does not have to be related to whether or not reconnection actually occurred earlier during propagation given the expected large spatial and temporal changes in plasma and magnetic field properties (e.g., shear angle, β) across the boundaries from the Sun to 1 AU. Similarly, the in situ observation of magnetic reconnection at the boundaries at 1 AU does not necessarily imply a large amount of erosion (e.g., if reconnection at a given MC only occurred late during propagation to 1 AU, the estimated erosion would be small). Finally, as noted by Wang et al. (2012), the criteria we used for identifying magnetic reconnection (mainly bifurcated current sheets and Walén test) are likely not unique; reconnection and erosion may be at work despite the lack of such signatures.

6. Conclusion

In this statistical study, we analyzed 109 MCs observed by Wind, 78 by STEREO-A, and 76 by STEREO-B during the period 1995 – 2012, on the basis of published lists. Due to the importance of reliable boundary determination in the implementation of the methods, we investigated in detail each event to define the MC boundaries with the best accuracy. Once the different key parameters (axis orientation, amount of eroded azimuthal magnetic flux at the front or rear boundaries, MC velocity, ΔV at boundaries) were calculated, we performed a selection based on important parameters such as MC quality (from boundary identification), impact parameter, ratio of eigenvalues from MVA and geometrical considerations (angle λ which determines the MC trajectory through the MC). Our analysis also focused on finding potential local reconnection exhausts at the MC boundaries, which also required classification depending on the quality of the signatures.

The main findings of the present study are as follows:

- The analysis of azimuthal flux imbalance in MCs at 1 AU suggests that erosion by magnetic reconnection is a frequent process.
- It suggests erosion can occur either at the front or at the rear, and in similar proportions.
- The absolute value of the amount of azimuthal magnetic flux is significant, albeit with significant uncertainties: on average 42 % at the front and 33% at the rear (relative to the total azimuthal flux content).
- These results are consistent with the frequent (up to ~30%) observation of reconnection exhausts locally at both the front and rear boundaries. This is particularly strengthened by the fact that the observations are from 1 AU, where conditions are not as favorable to reconnection as closer to the Sun where the plasma β is lower.
- Fitting MCs pre-supposing an axisymmetric geometry is not adapted to analyze erosion, which by assumption creates an asymmetric magnetic structure. Flux rope fitting thus should not be used to study erosion.
- The erosions estimated in the present study do not seem to be linked to solar wind and MC parameters as measured at 1 AU. The main reason is likely that parameters at 1 AU are not representative of the solar wind conditions that prevailed during the propagation of the MC between the Sun and 1 AU.

Azimuthal flux imbalance and local reconnection signatures thus consistently suggest that erosion is frequent and substantial. However, the flux imbalance analysis relies on methods which have significant potential drawbacks, in particular when impact parameters are large (for total flux estimate) and when the actual erosion is large (which impacts MVA and FRF determination of the main axis). Further quantification of the erosion process and of the impact of the limitations of the methods used here will require much larger MC datasets. In the future, it will also be interesting to investigate this process closer to the Sun based on data from Solar Orbiter, Solar probe Plus, and Bepi Colombo.

Acknowledgements. All the data are available through the NASA/GSFC's Space Physics Data Facility's CDAWeb service (www.cdaweb.gsfc.nasa.gov). The authors thank the Wind and STEREO teams for their work on instrument design, building and calibration. A. R. and B. L. are grateful to M. Janvier for fruitful discussions. Work at UNH is supported by NASA grants NNX10AQ29G, NNX13AP39G, and STEREO-FARSIDE.

References

Acuña, M. H., D. Curtis, J. L. Scheifele, C. T. Russell, P. Schroeder, A. Szabo, J. G. Luhmann (2008), The STEREO/IMPACT Magnetic Field Experiment, *Space Science Reviews*, *136*, 203-226, doi:10.1007/s11214-007-9259-2.

Borovsky, J. E., and M. Hesse (2007), The reconnection of magnetic fields between plasmas with different densities: Scaling relations, *Phys. Plasmas*, 14, 102309, doi:10.1063/1.2772619.

Burlaga, L.F., E. Sittler, F. Mariani, and R. Schwenn (1981), Magnetic loop behind an interplanetary shock: Voyager, Helios, and IMP 8 observations, *J. Geophys. Res.*, 86(A8), 6673–6684, doi:10.1029/JA086iA08p06673.

Burlaga, L. F. (1988), Magnetic Clouds and Force-Free Fields with Constant Alpha, *J. Geophys. Res., 93(A7*), 7217–7224, doi:10.1029/JA093iA07p07217.

Cartwright, M. L., & Moldwin, M. B. (2008), Comparison of small-scale flux rope magnetic properties to large-scale magnetic clouds: Evidence for reconnection across the HCS?, *J. Geophys. Res.,* 113, A09105, doi:10.1029/2008JA013389.

Cassak, P. A., and M. A. Shay (2007), Scaling of asymmetric magnetic reconnection: General theory and collisional simulations, *Phys. Plasmas*, 14, 102114, doi:10.1063/1.2795630.

Dasso, S., C. H. Mandrini, 5. Démoulin, M. L. Luoni (2006), A new model-independent method to compute magnetic helicity in magnetic clouds, *Astronomy and Astrophysics*, 455, 349-359, doi:10.1051/0004-6361:20064806.

Dasso, S., M. S. Nakwacki, P. Demoulin, and C. H. Mandrini (2007), Progressive transformation of a flux rope to an ICME, *Sol. Phys.*, 244(1–2), 115–137, doi:10.1007/s11207-007-9034-2.

Démoulin, P., and S. Dasso (2009), Magnetic cloud models with bent and oblate cross-section boundaries, *Astronomy and Astrophysics*, 507(2), 969-980, doi:10.1051/0004-6361/200912645.

Démoulin P., S. Dasso and M. Janvier (2013), Does spacecraft trajectory strongly affect detection of magnetic clouds?, *A&A,* 550 A3, DOI: http://dx.doi.org/10.1051/0004-6361/201220535

Farrugia, C., I. Richardson, L. Burlaga, R. Lepping, and V. Osherovich (1993), Simultaneous observations of solar MeV particles in a magnetic cloud and in the Earth's northern tail lobe: implications for the global field line topology of magnetic clouds and for the entry of solar particles into the magnetosphere during cloud passage, *J. Geophys. Res*., 98(A9), 15497–15.

Farrugia, C. J., L.F. Burlaga, and R. P. Lepping (1997), Magnetic Clouds and the quiet/storm effect at Earth: A review, in Magnetic Storms, Geophysical Monogr. Ser., vol. 98, pp. 91, edited by B. T Tsurutani, W. D. Gonzalez, Y. Kamide, and J. K. Arballo, AGU, Washington, D. C..

Feng, H. Q., Wu, D. J., Lin, C. C., Chao, J. K., Lee, L. C., & Lyu, L. H. (2008), *J. Geophys. Res.*, 113, A12105

Fenrich, F. R., and J. G. Luhmann (1998), Geomagnetic response to magnetic clouds of different polarity, *Geophys. Res. Lett*., 25(15), 2999-3002.

Galvin, A. B. et al. (2008), The Plasma and Suprathermal Ion Composition (PLASTIC) Investigation on the STEREO Observatories, *Space Science Reviews*, *136*(1-4), 437-486, doi:10.1007/s11214-007-9296-x.

Goldstein, H. (1983), On the field configuration in magnetic clouds, in Solar Wind Five, edited by Neugebauer, M., *NASA Conf. Publ*., CP-2280, 731–733.

Gosling, J. T., S. J. Bame, D. J. McComas, and J. L. Phillips (1990), Coronal mass ejections and large geomagnetic storms, *J. Geophys. Res*., 17(7), 901–904.

Gosling, J. T., R. M. Skoug, D. J. McComas, and C. W. Smith (2005), Direct evidence for magnetic reconnection in the solar wind near 1 AU, *J. Geophys. Res.*, 110, A01107, doi:10.1029/2004JA010809.

Gosling, J. T., S. Eriksson, R. Schwenn (2006), Petschek-type magnetic reconnection exhausts in the solar wind well inside 1 AU: Helios, *J. Geophys. Res*., 111, A10102, doi:10.1029/2006JA011863.

Gosling, J. T. (2011), Magnetic Reconnection in the Solar Wind, *Space Sci. Rev.*, *172*(1-4), 187–200, doi:10.1007/s11214-011-9747-2.

Gulisano, A., S. Dasso, C. Mandrini, and P. Démoulin (2007), Estimation of the bias of the minimum variance technique in the determination of magnetic clouds global quantities and orientation, *Adv. Space Res*., 40, 1881–1890, doi:10.1016/j.asr.2007.09.001.

Hudson, P. D. (1970), Discontinuities in an anisotropic plasma and their identification in the solar wind, *Planet. Space Sci.,* 19, 1161.

Janvier, M. P. Démoulin and S. Dasso, Global axis shape of magnetic clouds deduced from the distribution of their local axis orientation, *A&A* ,556 A50 (2013), DOI : http ://dx.doi.org/10.1051/0004-6361/201321442.

Janoo, L., C. J. Farrugia, R. B. Torbert, J. M. Quinn, A. Szabo, R. P. Lepping, K. W. Ogilvie, R. P. Lin, D. Larson, J. D. Scudder, V. A. Osherovich, and J. T. Steinberg (1998), Field and flow perturbations in the October 18-19, 1995 magnetic cloud, J. Geophys. Res., 103, 17,249.

Jian, L.K., C.T. Russell, J.G. Luhmann, A.B. Galvin, and K.D.C. Simunac (2013), Solar Wind Observations at STEREO: 2007-2011, *Amer. Inst. Phys. Proceedings of Solar Wind* 13, 1539, 191, doi: 10.1063/1.4811020.

Kaiser, M. L., T. A. Kucera, J. M. Davila, O. C. St. Cyr, M. Guhathakurta, E. Christian (2008), The STEREO Mission: An Introduction, *Space Science Reviews*, 136(1-4), 5-16, doi:10.1007/s11214-007-9277-0.

Kawano, H., and T. Higuchi (1995), The bootstrap method in space physics: Error estimation for the minimum variance analysis, *Geophys. Res. Lett*., 22(3), 307–310, doi:10.1029/94GL02969.

Klein, L. W., and L. F. Burlaga (1982), Interplanetary magnetic clouds at 1 AU, *J. Geophys. Res*., 87(A2), 613-624, doi:10.1029/JA087iA02p00613.

Lavraud, B., J. T. Gosling, A. P. Rouillard, A. Fedorov, A. Opitz, J.-A. Sauvaud, C. Foulllon, I. Dandouras, V. Génot, C. Jacquey, P. Louarn, C. Mazelle, E. Penou, T. D. Phan, D. Larson, J. G. Luhmann, P. Schroeder, R. M. Skoug, J. T. Steinberg and C. T. Russell (2009), Observation of a complex solar wind reconnection exhaust from spacecraft separated by over 1800 RE, *Solar Phys*., 256, No. 1-2, p. 379-392, doi:10.1007/s11207-009-9341-x.

Lavraud, B., A. Ruffenach, A. P. Rouillard, P. Kajdic, W. B. Manchester, and N. Lugaz (2014), Geo-effectiveness and radial dependence of magnetic cloud erosion by magnetic reconnection, *J. Geophys. Res. Space Physics*, 119, 26–35, doi:10.1002/2013JA019154.

Lepping, R. P., J. A. Jones, L. F. Burlaga (1990), Magnetic Field Structure of Interplanetary Magnetic Clouds at 1 AU, *J. Geophys. Res.*, 95(A8), 11,957–11,965, doi:10.1029/JA095iA08p11957.

Lepping, R.P., et al. (1995), The wind magnetic field investigation, *Space Sci. Rev*,71, 207-229.

Lepping, R. P., C.-C. Wu, and D. B. Berdichevsky (2005), Automated Identification of Magnetic Clouds and Cloud-like Regions at 1 AU: Occurrence Rate and Other Properties, *Ann. Geophysicae,* 23, 2687-2704.

Lepping, R. P., D. B. Berdichevsky, C.-C. Wu, A. Szabo, T. Narock, F. Mariani, A. J.

Lazarus, and A. J. Quivers (2006), A Summary of WIND Magnetic Clouds for the Years 1995 - 2003: Model-Fitted Parameters, Associated Errors, and classifications, *Annales Geophysicae*, 24(no. 1), 215-245.

Lin, R. P., et al. (1995), A three-dimensional plasma and energetic particle investigation for the Wind spacecraft, *Space Sci. Rev*., 71, 125.

Lopez, R. E. (1987), Solar cycle invariance in solar wind proton temperature relationships, *J. Geophys. Res.,* 92, 11.

Luhmann, J. G. et al. (2008), STEREO IMPACT Investigation Goals, Measurements, and Data Products Overview, *Space Science Reviews*, *136*(1-4), 117-184, doi:10.1007/s11214-007-

9170-x.
Lundquist, S. (1950), Magneto-hydrostatic fields. *Arkiv Fysik*, Bd 2, nr 35.
Mandrini C. H., M. S. Nakwacki, G. Attrill, L. van Driel-Gesztelyi, P. Démoulin, S. Dasso, H. Elliott (2007), Are CME-Related Dimmings Always a Simple Signature of Interplanetary Magnetic Cloud Footpoints?, *Solar Physics,* Volume 244, Issue 1-2, pp 25-43
McComas, D. J., J. T. Gosling, D. Winterhalter, and E. J. Smith (1988), Interplanetary magnetic field draping about fast coronal mass ejecta in the outer heliosphere, *J. Geophys. Res.*, 93(A4), 2519–2526, doi:10.1029/JA093iA04p02519.
McComas, D., S. Bame, P. Barker, W. Feldman, J. Phillips, P. Riley, and J. Griffee (1998), Solar Wind Electron Proton Alpha Monitor (SWEPAM) for the Advanced Composition Explorer, *Space Science Reviews*, 86(1), 563-612.
Möstl, C., C. Miklenic, C. J. Farrugia, M. Temmer, A. Veronig, A. B. Galvin, and H. K. Biernat (2008), Two-spacecraft reconstruction of a magnetic cloud and comparison to its solar source, *Ann. Geophys.,* 26, 3139–3152, doi:10.5194/angeo-26-3139-2008.
Nakwacki, M., S. Dasso, C. Mandrini, and P. Démoulin (2008); Analysis of large scale MHD quantities in expanding magnetic clouds, *Journal of Atmospheric and Solar-Terrestrial Physics*, *70*(10), 1318-1326, doi:10.1016/j.jastp.2008.03.006.
Owens, M. J., P. Démoulin, N. P. Savani, B. Lavraud, and A. Ruffenach (2012), Implications of non-cylindrical flux ropes for magnetic cloud reconstruction techniques and the interpretation of double flux-rope events, *Sol. Phys*., 278(2), 435–446, doi:10.1007/s11207-012-9939-2.
Phan, T. D., et al. (2006), A magnetic reconnection X-line extending more than 390 Earth radii in the solar wind, *Nature*, 439(7073), 175–178, doi:10.1038/nature04393.
Paschmann, G., I. Papamastorakis, W. Baumjohann, N. Sckopke, C. W. Carlson, B. U. Ö. Sonnerup, and H. Lühr (1986), The Magnetopause for Large Magnetic Shear: AMPTE/IRM Observations, *J. Geophys. Res.*, 91(A10), 11,099–11,115, doi:10.1029/JA091iA10p11099.
Riley, P., J.A. Linker, R. Lionello, Z. Mikić, D. Odstrcil, M.A. Hidalgo, C. Cid, Q. Hu, R.P. Lepping, B.J. Lynch, A. Rees (2004), Fitting flux ropes to a global MHD solution: a comparison of techniques, Journal of Atmospheric and Solar-Terrestrial Physics, Volume 66, Issue 15-16, p. 1321-133, doi: 10.1016/j.jastp.2004.03.019
Rouillard, A. P., B. Lavraud, N. R. Sheeley, J. a. Davies, L. F. Burlaga, N. P. Savani, C. Jacquey, and R. J. Forsyth (2010), White Light and in Situ Comparison of a Forming Merged Interaction Region, *The Astrophysical Journal*, *719*(2), 1385-1392, doi:10.1088/0004-637X/719/2/1385.
Ruffenach, A., et al. (2012), Multispacecraft observation of magnetic cloud erosion by magnetic reconnection during propagation, *J. Geophys. Res*., 117, A09101, doi:10.1029/2012JA017624.
Sauvaud, J.-A, D. Larson, C. Aoustin, D. Curtis, J.-L. Médale, A. Fedorov, J. Rouzaud, et al. (2008), The IMPACT Solar Wind Electron Analyzer (SWEA*), Space Science Reviews*, 136, 227-239, doi:10.1007/s11214-007-9174-6.
Savani, N. P., M. J. Owens, A. P Rouillard., R. J. Forsyth, K. Kusano, D. Shiota, R. Kataoka (2011), Evolution of Coronal Mass Ejection Morphology with Increasing Heliocentric Distance. I. Geometrical Analysis, *The Astrophysical Journal*, Volume 731, Issue 2, doi:10.1088/0004-637X/731/2/109
Savani, N. P., M. J. Owens, A. P Rouillard., R. J. Forsyth, K. Kusano, D. Shiota, R. Kataoka, L. Jian, V. Bothmer (2011), Evolution of Coronal Mass Ejection Morphology with Increasing Heliocentric Distance. II. In Situ Observations, *The Astrophysical Journal*, Volume 732, Issue 2, article id. 117, doi: 10.1088/0004-637X/732/2/117
Savani, N. P., A. Vourlidas, D. Shiota, M. G. Linton, K. Kusano, N. Lugaz, A.P. Rouillard (2013), A Plasma β Transition within a Propagating Flux Rope, *The Astrophysical Journal*, Volume 779, Issue 2, article id. 142, doi: 10.1088/0004-637X/779/2/142

Sonnerup, B.U.Ö., Scheible, M., (1998), Minimum and maximum variance analysis. In: Pashmann, G., Daly, P.W. (eds.) *Analysis Methods for Multi-Spacecraft Data*, ISSI Scientific Report SR-001, Bern, Chap. 8, 185.

Swisdak, M., et al. (2010), The vector direction of the interstellar magnetic field outside the heliosphere, *Ap. J.,* 710, doi:10.1088/0004-637X/710/1769.

Tian, H., S. Yao, Q. Zong, J. He, and Y. Qi (2010), Signatures of Magnetic Reconnection At Boundaries of Interplanetary Small-Scale Magnetic Flux Ropes, *Astrophys. J.*, *720*(1), 454–464, doi:10.1088/0004-637X/720/1/454.

Wang et al. (2012), Variations of solar electron and proton flux in magnetic cloud boundary layers and comparisons with those across the shocks and in the reconnection exhausts, Astrophys. J.,749, 82, doi : 10.1088/0004-637X/749/1/82.

Wei, F., R. Liu, Q. Fan, and X. Feng (2003), Identification of the magnetic cloud boundary layers*, J. Geophys. Res.,* 108, 1263, doi:10.1029/2002JA009511, A6.

WIND	Front boundaries		Rear boundaries	
Reconnection signatures of…	For 53 MCs Q1	For 30 MCs Q2F	For 53 MCs Q1	For 7 MCs Q2R
Category 1	3	1	9	0
Category 2	4	6	6	0
Category 3	1	0	1	1

STEREO-A	Front boundaries		Rear boundaries	
Reconnection signatures of…	For 37 MCs Q1	For 7 MCs Q2F	For 37 MCs Q1	For 1 MCs Q2R
Category 1	9	3	10	0
Category 2	13	2	11	1

STEREO-B	Front boundaries		Rear boundaries	
Reconnection signatures of…	For 30 MCs Q1	For 16 MCs Q2F	For 30 MCs Q1	For 4 MCs Q2R
Category 1	11	5	6	3
Category 2	5	3	8	0

Table 1. Summary of magnetic reconnection signatures observed at the front and rear boundaries of the MCs, as a function of category. Only well-determined MC boundaries were analyzed (cf. section 4.3).

(a)	Group MVA		Group FRF	
	MC eroded at the front	MC eroded at the rear	MC eroded at the front	MC eroded at the rear
Number of MCs	23	27	19	26
Average rate of eroded Azimuthal flux (%)	42 (23/5)	33 (26/5)	24 (15/3)	28 (18/4)
Average Azimuthal eroded flux (*10^{21} Mx/UA)	1.07 (0.92/0.20)	0.90 (1.61/0.31)	0.38 (0.35/0.08)	0.62 (0.74/0.15)
Average velocity of MCs (km/s)	381.4 (52.2/10.9)	452.7 (152.5/29.3)	417.9 (72.3/16.6)	426.8 (119.4/23.4)
ΔV_{front} mean (km/s)	52.8 (40.4/8.4)	96.3 (135.1/26.0)	54.2 (78.2/17.9)	58.9 (69.0/13.5)
ΔV_{rear} mean (km/s)	-29.4 (46.5/9.7)	-16.0 (56.7/10.9)	-51.3 (54.6/12.5)	-23.8 (46.3/9.1)
$Valfvén_{front}$ (km/s)	46.3 (21.0/4.4)	70.7 (40.2/7.8)	64.5 (52.0/11.9)	88.1 (117.9/23.1)
$Valfvén_{rear}$ (km/s)	67.4 (40.6/8.5)	71.3 (49.1/9.4)	68.2 (36.7/8.4)	64.6 (61.2/12.0)

(b)	Group MVA*		Group FRF*	
	MC eroded at the front	MC eroded at the rear	MC eroded at the front	MC eroded at the rear
Number of MCs	44	36	35	44
Average amount of eroded azimutal flux (%)	44 (25/4)	33(23/4)	23 (15/3)	31 (20/3)
Average azimuthal eroded flux ($*10^{21}$ Mx/UA)	1.13 (1.14/0.17)	0.95 (1.60/0.27)	0.32 (0.29/0.05)	0.53 (0.69/0.10)
Average velocity of MCs (km/s)	406.9 (71.7/10.8)	471.1 (151.0/25.2)	419.9 (66.8/11.3)	425.5 (133.2/20.1)
ΔV_{front} mean (km/s)	50.4 (52.1/7.9)	107.2 (126.6/21.6)	40.2 (74.5/12.6)	67.9 (74.8/11.3)
ΔV_{rear} mean (km/s)	-31.5 (59.2/8.9)	-14.0 (59.2/7.9)	-49.4 (59.8/10.1)	-27.0 (48.9/7.4)
$Valfvén_{front}$ (km/s)	64.4(51.0/7.7)	76.0 (43.2/7.2)	61.8 (40.8/7.4)	76.7 (90.6/13.8)
$Valfvén_{rear}$ (km/s)	67.5 (67.2/10.1)	69.0.3 (34.9/5.8)	81.8(74.0/12.7)	67.3 (43.3/6.6)

Table 2. Average parameters estimated for groups (a) MVA and FRF defined in Section 4.1, and (b) MVA* and FRF* defined in Section 4.2. The standard deviation, σ, is indicated in brackets with the uncertainty on the average $\sigma/\sqrt{n}$ where n is the size of the sample. The lines are: (1) number of MCs in each group by splitting MCs eroded at the front and those eroded at the rear; (2) Average (percentage) amount of eroded azimuthal flux for each category; (3) Average azimuthal magnetic flux eroded ($*10^{21}$ Mx/UA) from the direct method [*Dasso et al*., 2006]; (4) Average velocity of MCs (km/s); (5) $\Delta V_{front}=V_{MC}-V_{sw,front}$, where the ambient solar wind ($V_{sw,front}$) is the local proton speed at the MC front and ahead of the shock if present, and V_{MC} is the average of proton speed in the first 5% of the MC; (6) $\Delta V_{rear}=V_{MC}-V_{sw,rear}$ where $V_{sw,rear,}$ is the highest speed in the 6 hour interval following the MC based on 30 min average and V_{MC} is the average proton speed in the last 5% of the MC; (7 and 8) hybrid Alfvén speed at MC front and rear boundaries (cf. section 4.2)

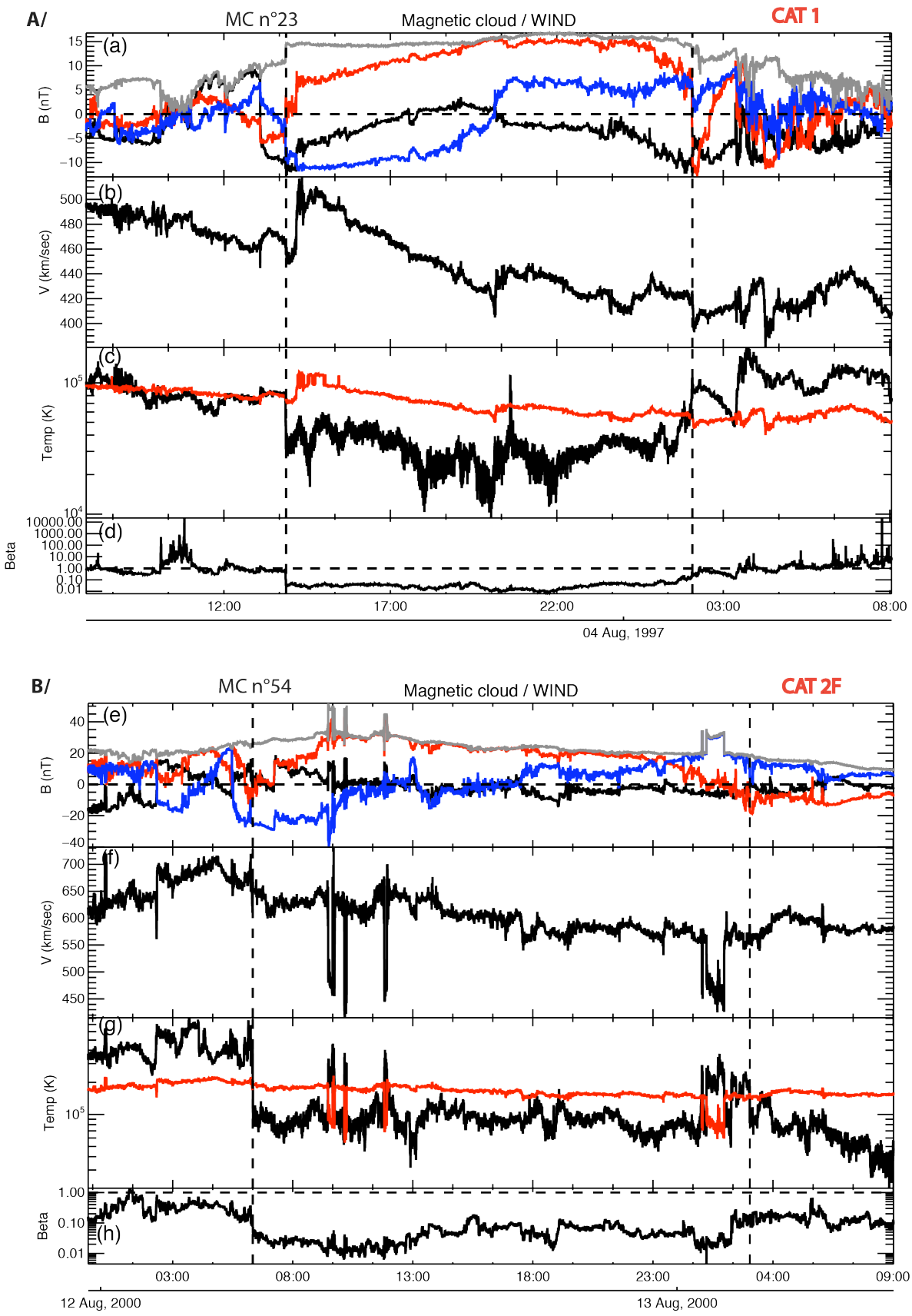


Figure 1. Plasma and magnetic field data from WIND for 2 illustrative MCs on (a) August 3 1997 and (b) August 12 2000. MC boundaries are indicated with dashed lines. The panels show: (a,e) magnetic field components in GSE coordinates (|B| gray, B_x black, B_y red, B_z blue), (b,f) the proton velocity magnitude, (c,g) proton temperature observed (black line) and predicted (in red) by the empirical relation of Lopez et al. [1987], and (d,h) proton β.

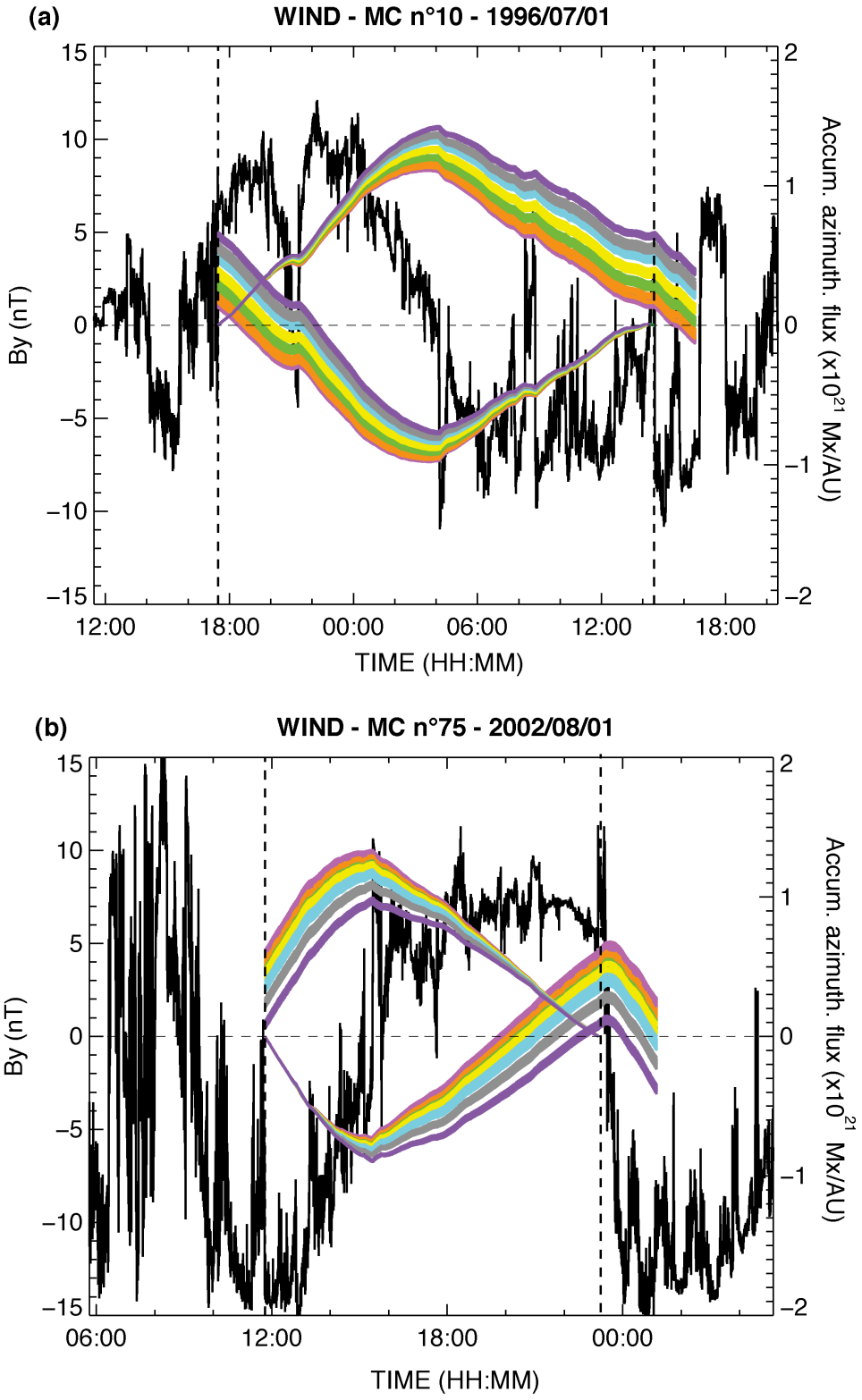
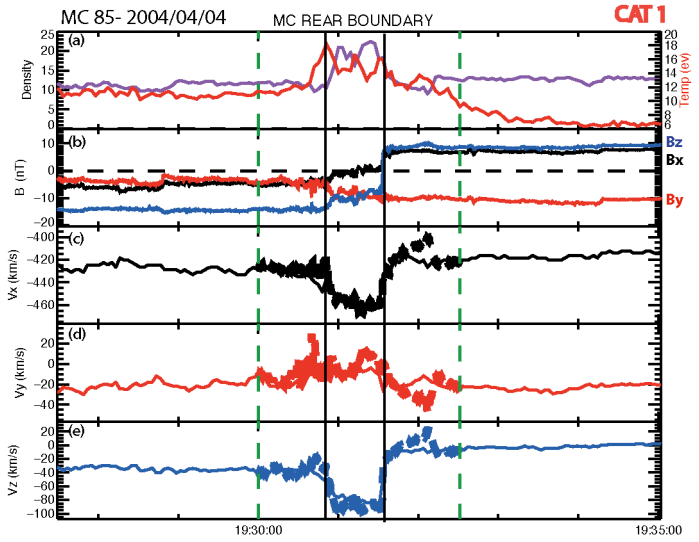
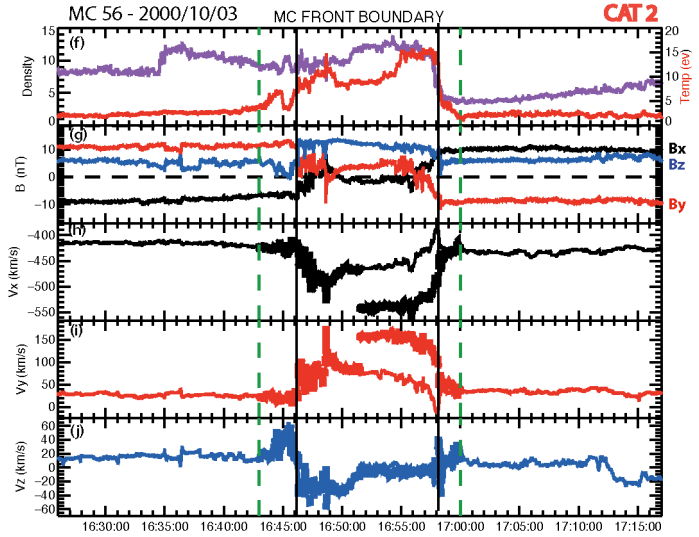


Figure 2. $B_{y,cloud}$ magnetic component (black line) and accumulative azimuthal magnetic flux per unit length for (a) MC n°10 on 1 July 1996 and (b) MC n°75 on 1 August 2002, both observed by WIND. The colored curves show the results in accumulative flux by using axis orientations from MVA, with the "nested-bootstrap" method (cf. Section 4.1 for details). A set of curves comes from the integration of $B_{y,cloud}$ starting at the front boundary while for the second set the integration starts at the rear boundary. For MC n°10 (panel a), the variations are consistent with erosion at the rear of the MC, so that excess azimuthal magnetic flux is present at the front, and conversely for MC n°75 (panel b).


MC 85- 2004/04/04
MC REAR BOUNDARY
CAT 1
Density
Temp (ev)
B (nT)
Bz
Bx
By
Vx (km/s)
Vy (km/s)
Vz (km/s)
19:30:00
19:35:00


MC 56 - 2000/10/03
MC FRONT BOUNDARY
CAT 2
Density
Temp (ev)
B (nT)
Bx
Bz
By
Vx (km/s)
Vy (km/s)
Vz (km/s)
16:30:00
16:35:00
16:40:00
16:45:00
16:50:00
16:55:00
17:00:00
17:05:00
17:10:00
17:15:00

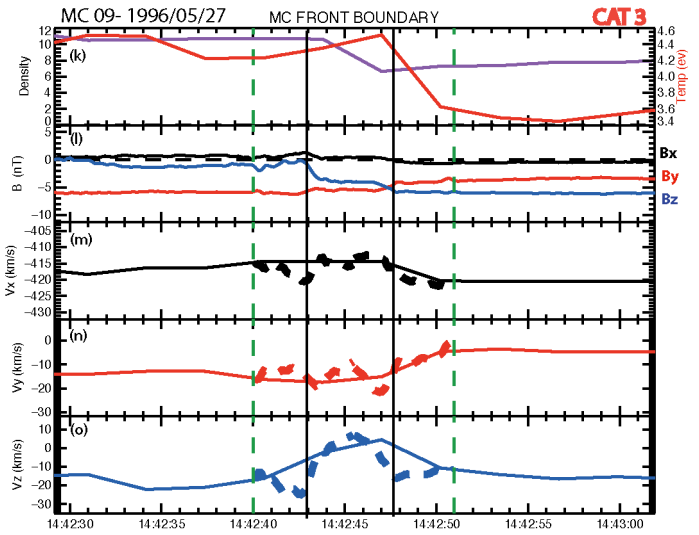

MC 09- 1996/05/27
MC FRONT BOUNDARY
CAT 3
Density
Temp (ev)
B (nT)
Bx
By
Bz
Vx (km/s)
Vy (km/s)
Vz (km/s)
14:42:30
14:42:35
14:42:40
14:42:45
14:42:50
14:42:55
14:43:00

Figure 3. Plasma data from WIND for a selected set of 3 MC boundaries, together with Walén test results: (a) MC n°85 (2004/04/04), (b) n°56 (2000/03/10), (c) n°9 (1996/05/27). Each case illustrates a different category (1 through 3) in magnetic reconnection signature (cf section 3). The panels show (a,f,k) density and proton temperature, and (b,g,l) magnetic field components (in GSE coordinates). The remaining panels display the components of the observed and predicted (from Walén relation) velocity vectors (GSE coordinate system). Green vertical lines denote the reference times for the Walén test (which is performed "inward"). The vertical black lines denote the edges of the exhaust, i.e., the bifurcated current sheets.

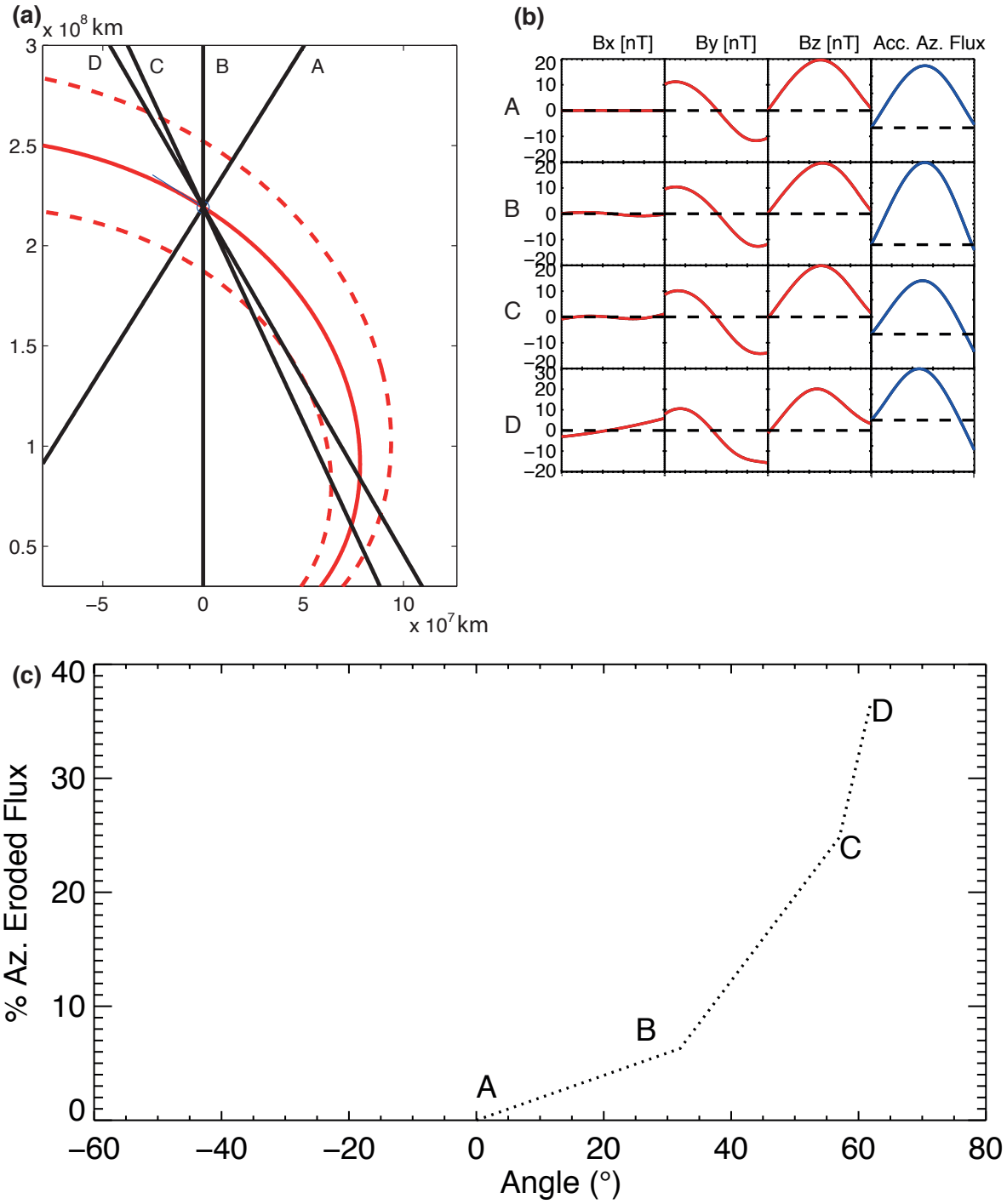


Figure 4. Impact of spacecraft trajectory through a MC (a) on the asymmetry in azimuthal magnetic flux (b), and inferred impact on the estimated eroded magnetic flux from the direct method of *Dasso et al.* [2006]. (a) Illustration of several virtual spacecraft crossings (black lines) through a model MC. The model is a flux tube with a cylindrical geometry whose axis is curved along a Parker spiral direction (c.f. *Owens et al. [2012]*). This figure displays the MC central axis and outer boundaries in the ecliptic plane, The Sun center is at coordinate (0;0) on the graph (where the red lines originate). The angles of the normal to the main axis orientation relative to the trajectory at the point of crossing are respectively 0, 32, 57, and 62°. (b) Variations in magnetic field components (nT) as simulated along the spacecraft trajectory, in the MC coordinate system and the accumulative azimuthal magnetic flux from the integration of B_y (in Arbitrary Unit) for each crossing. (c) Variation of the amount of azimuthal flux eroded (%) as a function of the angle 0, 32, 57, and 62° (based on the four trajectories).

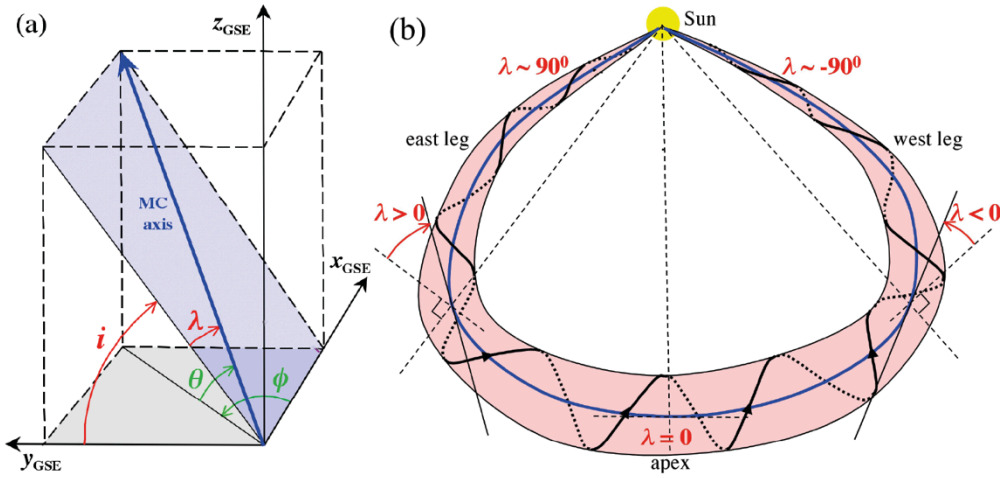


Figure 5. MC schematic with the angle λ et *i* as defined in Janvier et al. [2013]. (a) Definition of all angles in GSE coordinate system relative to the axis orientation including the angles, φ and θ. (b) Variation of the angle λ in the plane of the MC along the flux tube (cf. text for further details).

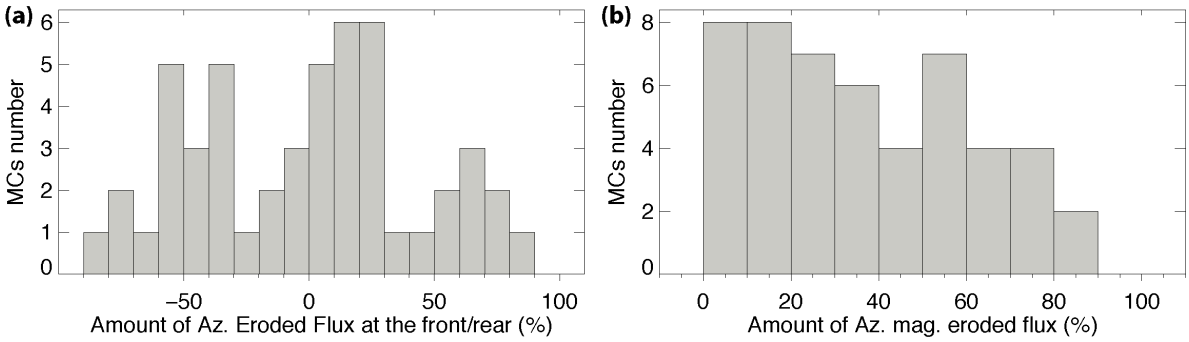


Figure 6. (a) Distribution of MCs from Group MVA as a function of the amount of eroded azimuthal magnetic flux at the front (-100 to 0%) and at the (0 to 100 %). (b) Distribution of Group MVA as a function of the absolute value of eroded azimuthal magnetic flux.

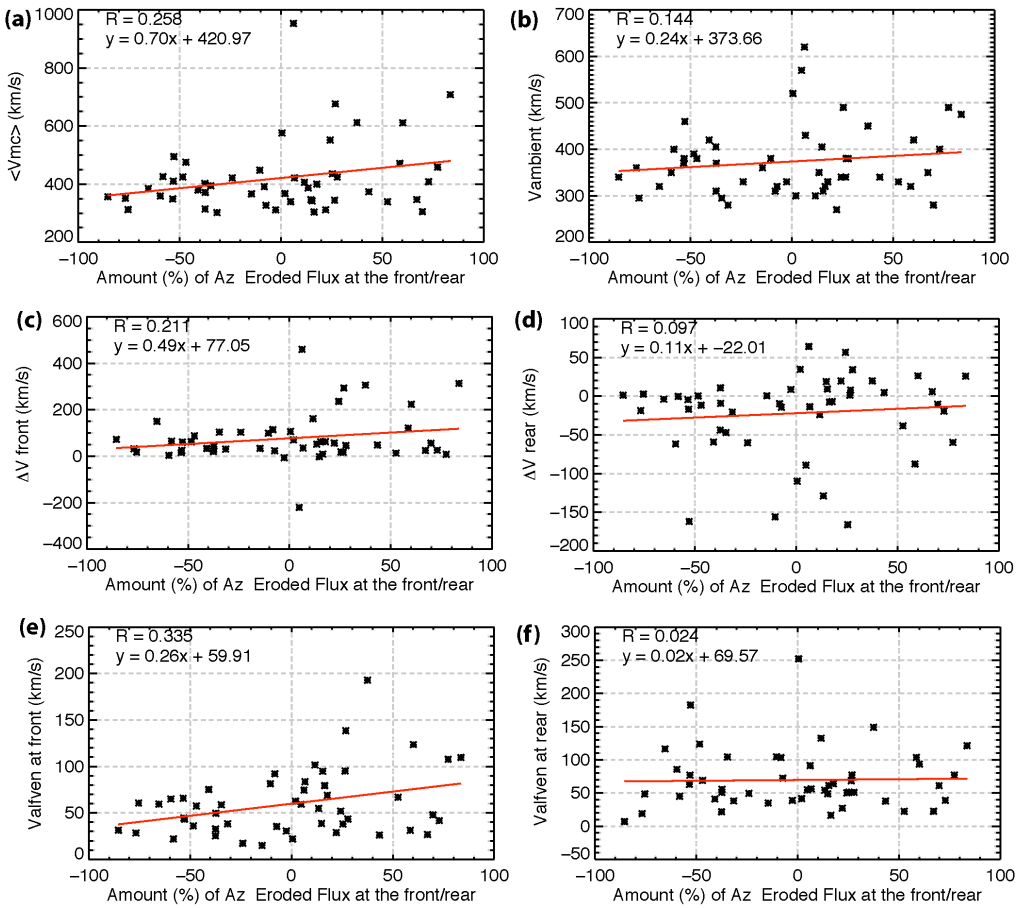


Figure 7. Results of the various correlation analyses performed for the set of MCs from group MVA, all as a function of the amount of eroded azimuthal magnetic flux. (a) Average speed of MCs $<V_{MC}>$, (b) ambient solar wind speed, (c/d) local variation in speed at the front or rear boundary (ΔV_{front}/ ΔV_{rear}), and (e/f) average Alfvén speed at front or rear boundary. The Pearson correlation coefficients (R) are indicated.

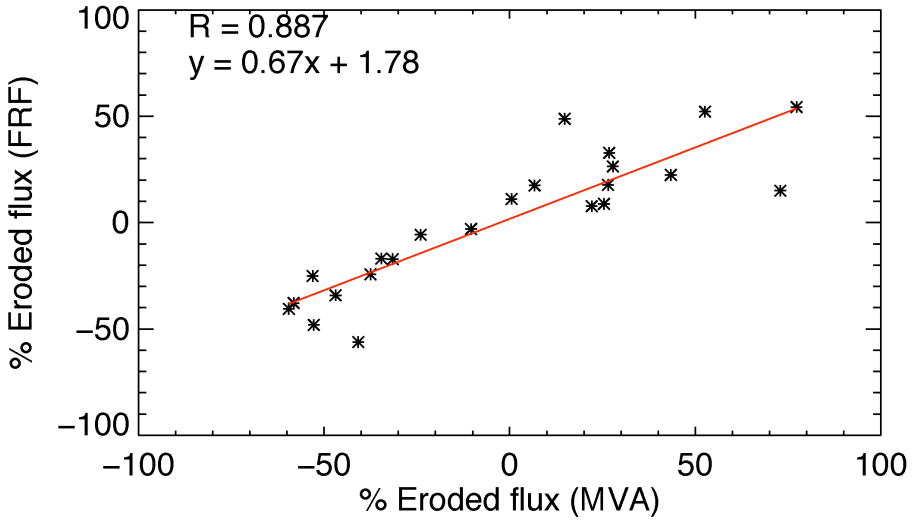


Figure 8. Variation of the amount of eroded azimuthal magnetic flux as determined using main axis determination from FRF as a function of that determined from the results of MVA. Only MCs simultaneously belonging to groups MVA and FRF are plotted. Erosion is systematically underestimated by 33% when using the results from FRF.